APPLIED SCIENCES AND ENGINEERING

Highly stable hybrid perovskite light-emitting diodes based on Dion-Jacobson structure

Yuequn Shang[1,2,3]*, Yuan Liao[1]*, Qi Wei[1]*, Ziyu Wang[1], Bo Xiang[1], Youqi Ke[1], Weimin Liu[1†], Zhijun Ning[1†]

Organic-inorganic hybrid halide perovskites are emerging as promising materials for next-generation light-emitting diodes (LEDs). However, the poor stability of these materials has been the main obstacle challenging their application. Here, we performed first-principles calculations, revealing that the molecule dissociation energy of Dion-Jacobson (DJ) structure using 1,4-bis(aminomethyl)benzene molecules as bridging ligands is two times higher than the typical Ruddlesden-Popper (RP) structure based on phenylethylammonium ligands. Accordingly, LEDs based on the DJ structure show a half-lifetime over 100 hours, which is almost two orders of magnitude longer compared with those based on RP structural quasi–two-dimensional perovskite. To the best of our knowledge, this is the longest lifetime reported for all organic-inorganic hybrid perovskites operating at the current density, giving the highest external quantum efficiency (EQE) value. In situ tracking of the film composition in operation indicates that the DJ structure was maintained well after continuous operation under an electric field.

INTRODUCTION

Metal halide perovskite is rising as a promising candidate for the next-generation light-emitting diodes (LEDs) due to its sharp emission peak, high luminescence quantum yield (QY), and solution processability (*1*, *2*). To enhance device performance, intense efforts were made in recent years for developing new perovskite materials (*3*–*7*) and device architectures (*8*–*10*), and much work were devoted to understanding the working mechanism (*11*, *12*). Through suppressing nonradiative recombination and balancing carrier injection (*13*, *14*), the luminescence efficiency of the device has been significantly improved. Up to now, the peak external quantum efficiency (EQE) of perovskite light-emitting devices exceeded 20% (*14*–*17*), which is comparable to organic LED (OLED) (*18*).

Despite a significant increase in efficiency, the development of perovskite LED is plagued for its poor stability. First, because of its soft structure, perovskite can easily decompose at high-temperature or high-humidity environment (*19*–*21*). Second, organic cations and halides can move under electric field, giving rise to the transformation of perovskite structure (*22*–*24*). As a result, the peak efficiency of many perovskite LEDs can only keep seconds or minutes under operation. Furthermore, ions moving under electric field can cause structural distortion, inducing luminescence wavelength shift (*25*). It is therefore imperative to improve the stability of perovskite materials and devices, as well as to clarify the device degradation mechanism.

In this work, we performed density functional theory (DFT) simulation to calculate the structural dissociation energies of quasi–two-dimensional (2D) Dion-Jacobson (DJ) structural perovskite using bidentate organic molecules 1,4-bis(aminomethyl)benzene (BAB) as bridging molecules and Ruddlesden-Popper (RP) structure using phenylethylamine (PEA). Both binding energy between the layered structures and molecule dissociation energy of the DJ structure are much higher than the RP structure. Then, a DJ structural perovskite–based LED (*26*–*28*) using bidentate organic molecules BAB as bridging molecules was fabricated. We tracked the stability of the device at the point of the highest EQE and observed T_{50} lifetime up to 100 hours, which is two orders of magnitude longer than that based on the RP structure based on PEA. Furthermore, no obvious change of the wavelength of the film was found after 100 hours of continuous operation. We characterized the perovskite structure after continuous operation using transient absorption (TA) measurement: No change of the DJ structure was found, in contrast to the obvious transformation of RP structure. In addition, an energy level landscape engineered quasi-2D structure was constructed by manipulating the composition of the film, bringing an EQE over 5%. This work raises the expectancy for developing highly stable and efficient perovskite LEDs.

RESULTS

Theoretical calculation

We performed DFT simulation to study the stability of DJ and RP structural quasi-2D perovskites using BAB and PEA as bridging molecules, respectively (Fig. 1A). RP structure, generally using a single amino group ligand, has a half lattice constant dislocation between two layered perovskites, whereas no dislocation is present for the DJ structure, typically using diamino group ligands (Fig. 1A). The calculated distance between the layered PbI_6 octahedral of DJ and RP structures are 1.15 and 1.65 nm, respectively, which is consistent well with the experimental results below (table S1). We then compared the binding energy of these two quasi-2D perovskites (Fig. 1B and fig. S2). Since BAB molecule contains two amino ending groups and both of them can bind with PbX_6 octahedrons, it only contains ionic binding between octahedron and amino groups with a binding energy of −131.4 meV Å^{-2}. In the case of PEA molecule–based quasi-2D perovskite, two molecules packed back to back were present between octahedral layers since it has only one amino group (Fig. 1A). For PEA-based quasi-2D perovskite, besides ionic binding between amino unit and octahedral structure, it has additional van der Waals binding between two PEA molecules with a binding energy of only −9.7 meV Å^{-2}. Because of this low binding energy between the two layers of PEA molecules, the layered perovskite is easy to dissociate, as shown in fig. S2.

[1]School of Physical Science and Technology, ShanghaiTech University, Shanghai 201210, China. [2]Shanghai Institute of Ceramics, Chinese Academy of Sciences, Shanghai 200050, China. [3]University of Chinese Academy of Sciences, Beijing 100049, China.
*These authors contributed equally to this work.
†Corresponding author. Email: liuwm@shanghaitech.edu.cn (W.L.); ningzhj@shanghaitech.edu.cn (Z.N.)

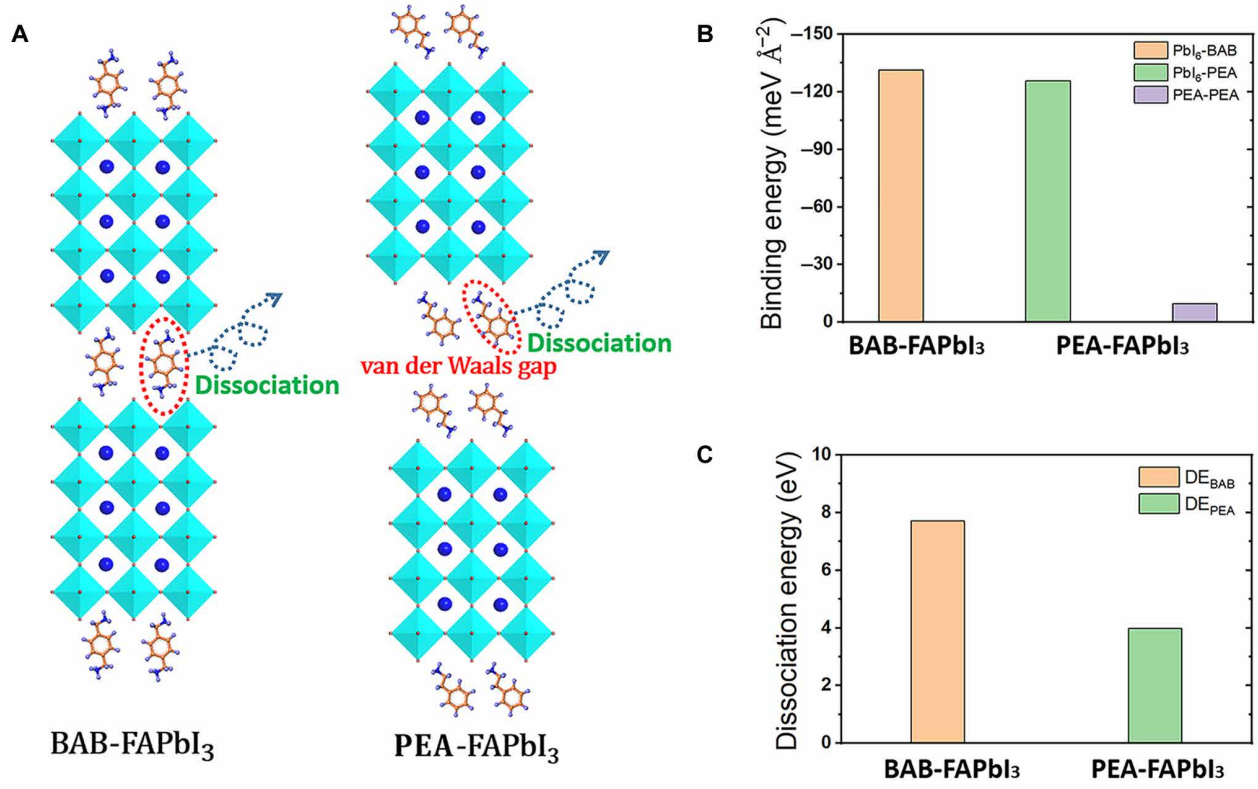

Fig. 1. DFT simulation of perovskites. (**A**) Schematic of four-layer structures of BAB-$FAPbI_3$ and PEA-$FAPbI_3$, dissociation of ligands, and van der Waals force between PEA molecules. (**B**) Calculated binding energies between PbI_6-BAB, PbI_6-PEA, and PEA-PEA. (**C**) Calculated molecule dissociation energy of the perovskites based on BAB and PEA.

The dissociation of ligand molecule is an important factor in inducing the decomposition of perovskite structure (*29*, *30*), thereby we calculated the dissociation energy (DE) of BAB and PEA in both perovskite structures (fig. S3). The dissociation energy of BAB is 7.684 eV, almost two times larger than PEA (3.988 eV; Fig. 1C), suggesting that PEA molecule is much easier to dissociate from the structure. The dissociation of surface passivation molecules can introduce oxygen and water into structure, leading to the further decomposition of PbI_6 scaffold (*29*, *30*).

Hybrid DJ structure perovskite

We used a typical one-step method to deposit hybrid DJ structure perovskite films using a precursor containing formamidinium iodide (FAI), PbI_2, and a varying amount of BAB bromide ($BABBr_2$) (*27*). The complete formula of the perovskite is given as (BAB) $FA_{n-1}Pb_nX_{3n+1}$(X = Br, I), where n represents the number of $FAPbX_3$ layers. For simplicity, we used the percentage of BAB in all organic molecules to name the material, for instance, the structure with $n = 3$ was named **BAB33** (Fig. 2A).

The absorption and photoluminescence (PL) results of the quasi-2D DJ structure perovskite **BAB33** are shown in Fig. 2B. The peak at 526 nm can be ascribe to a single-layer structure (*26*, *31*), while the other two peaks could derive from PbI_2 nanoparticles (*32*) or low-dimensional perovskite such as 0D and 1D structures (*4*). The normalized PL spectrum is plotted in Fig. 2B, and the DJ structure perovskite films show an emission peak at 750 nm and a large full width at half maximum (FWHM) value of more than 60 nm. The broad emission peak can be related to the radiation recombination from low-dimensional structures of different layer number. The PL QY as a function of the excitation intensity is plotted in Fig. 2C. PL QY is increased as the enhancement of illumination intensity since the probability of recombination decay is enhanced as the increase in carrier concentration (*3*).

The structure of the film was characterized by both x-ray diffraction (XRD) and grazing-incidence wide-angle x-ray scattering (GIWAXS). Hybrid DJ structure perovskite films exhibit diffraction peaks at near 14° and 30° in XRD spectrum (fig. S6), corresponding to (100) and (200) planes of 3D perovskite. We observe diffraction spots deriving from (001) plane of the 2D structure in the GIWAXS pattern at a beam angle of 0.2° (Fig. 3), indicating the presence of single-layer perovskite structure. For perovskite **BAB80**, the stronger spot oriented from (001) plane indicates that the ratio of the single-layer structure in the film is increased. Upon the decrease in BAB ratio, the spot becomes weak, showing that more multiple layer domains are formed (Fig. 3, A and B, and fig. S7, A to C). We measured the composition of the structure inside the film by increasing the beam angle to 1°. The appearance of the Debye-Scherrer ring generating from (100) plane of the single-layer structure indicates that the orientation of the layered structure is random inside the film (Fig. 3C and fig. S7, D to F).

For comparison, we tested RP phase perovskite films using naphthylmethylamine (NMA) and PEA as bridging ligands. We extracted the 1D x-ray scattering profiles along the q_z direction of all films from GIWAXS patterns (Fig. 3D and fig. S7, G and H). DJ structure perovskite with BAB as a separating ligand shows the smallest

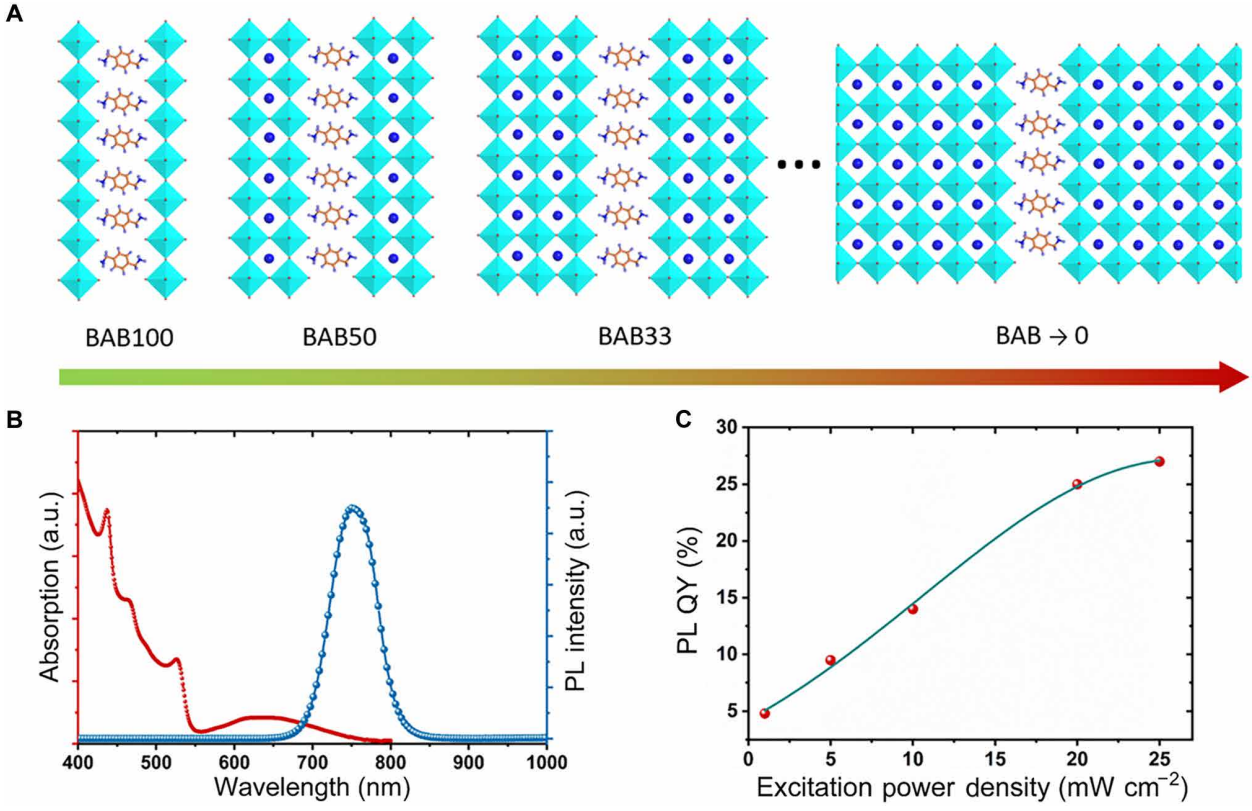

Fig. 2. Properties of DJ structure perovskite films. (**A**) Scheme of BAB-FAPbX$_3$ phases. The blue ball is FA, the cyan square is PbX$_6$ octahedron, and the molecule is BAB. (**B**) Absorption and photoluminescence (PL) of **BAB33** film. (**C**) Excitation intensity–dependent PL QY of **BAB33** film. a.u., arbitrary units.

diffraction peak located at $q = 0.55$ A^{-1}, corresponding to the ligands separated interplanar spacing of 1.13 nm, which is consistent well with the length of the BAB molecular layer based on theoretic simulation. The calculated interplanar distances of RP structural perovskites based on PEA and NMA ligands are 1.69 and 2.2 nm, respectively. The interplanar spacing of DJ structure based on BAB is two times smaller than that of RP structure based on NMA, suggesting that only one layer of molecules exist between the layered octahedral structure and both amino units are connected with PbX$_6$ octahedral structure.

Transient dynamics

High PL QY and effective carrier injection are important to get high-performance LEDs; they are closely related to the distribution of low-dimensional perovskite structure with varied layer values. To improve carrier transfer and PL QY, we tuned the composition of DJ structure via adding an extra amount of FA—the ratio of BAB to FA was reduced to 25% (**BAB25**) instead of 33% for **BAB33**. The decrease in the ratio of big molecules could result in the increase in ratio of multilayered structure in comparison to single-layer structure, since the n value of (BAB) $FA_{n-1}Pb_nX_{3n+1}$ is increased.

To reveal the composition of the film, we performed TA spectroscopy (TAS) measurements (Fig. 4). We observed several bleaching peaks related to the transient luminescence of the structures of varied n value. The negative band at 550 nm can be ascribed to transient luminescence for single-layer perovskite ($n = 1$), while the peaks between 600 and 750 nm are related to perovskites with multiple layers. For **BAB33**, the TAS bands between 600 and 750 nm are much weaker, relative to the peak at 550 nm (Fig. 4, A and B), indicating that the single-layer perovskite dominates the film. For the sample **BAB25**, the intensity of TAS bands between 600 and 750 nm is remarkably enhanced, suggesting that the ratio of DJ structures with multiple layers is increased (Fig. 4, C and D) (*3*). When BAB is replaced by PEA with the same amount of amino groups, the ratio of single-layer structure is increased according to TA spectra (fig. S8A). This can be ascribed to the fact that PEA is kinetically easier to form a layered structure since it only needs to form one ionic bond.

The energy transfer between perovskites of different layer number is analyzed on the basis of the evolution of TA spectra. For both **BAB25** and **BAB33**, the TAS signals exhibit a fast decay of the bleaching peak at 550 nm, followed by rise of the peaks between 600 and 750 nm, indicating energy transfer from single-layer structure to multilayered structures. For **BAB25**, the intensity of peaks between 600 to 750 nm is much higher than those of **BAB33**, suggesting that the carriers are more effectively transferred between different structures. The red shift due to energy transfer can be observed from the curves after global fitting (fig. S8, B and C), and the intensity of peaks belonging to multilayered structure of **BAB25** is almost doubled in comparison to that of **BAB33** film.

Device structure and performance

We then prepared LED based on DJ perovskite with structure of indium tin oxide (ITO)/ZnO/polyethylenimine ethoxylated (PEIE)/perovskites/poly-[(9,9-dioctylfluorenyl-2,7-diyl)-alt-(4,4′-(*N*-(4-butylphenyl) (TFB)/MoO_3/Al (Fig. 5A). Carrier-transporting layers

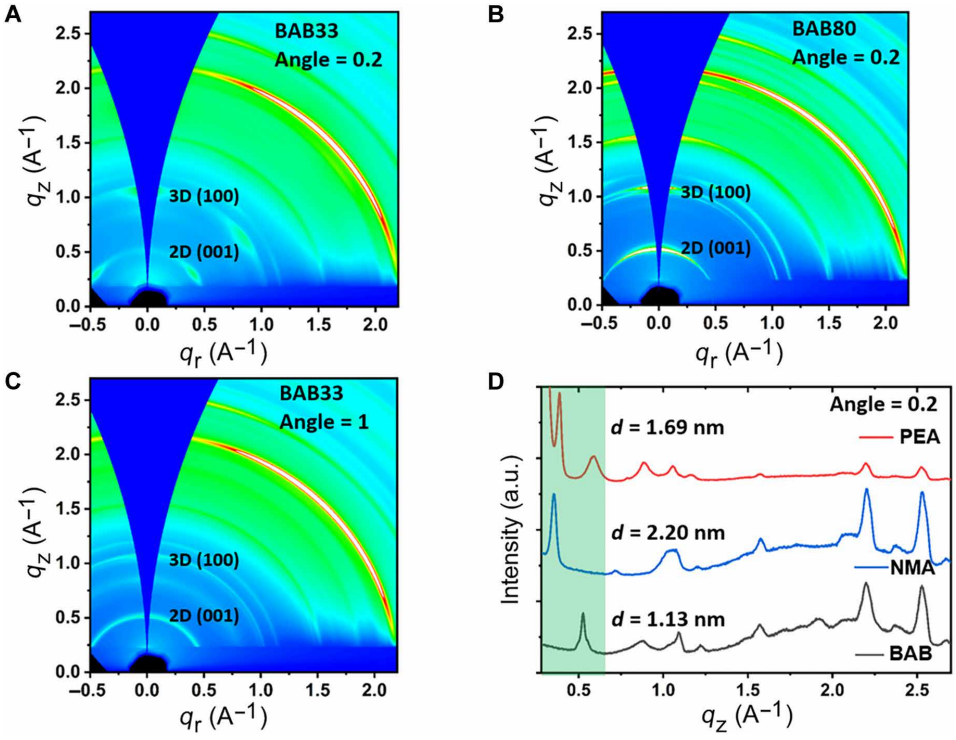

Fig. 3. GIWAXS pattern of perovskite films with varied ligands. (**A**) 33% and (**B**) 80% of BAB ligand (**BAB33** and **BAB80**, the incidence angles are 0.2°). (**C**) GIWAXS pattern of the **BAB33** perovskite film with incidence angles equal 1°. (**D**) XRD pattern from GIWAXS. The value of *q* can be obtained from the XRD pattern, and the corresponding interplane spacing *d* is 1.13, 1.69, and 2.20 nm for BAB, PEA, and NMA, respectively.

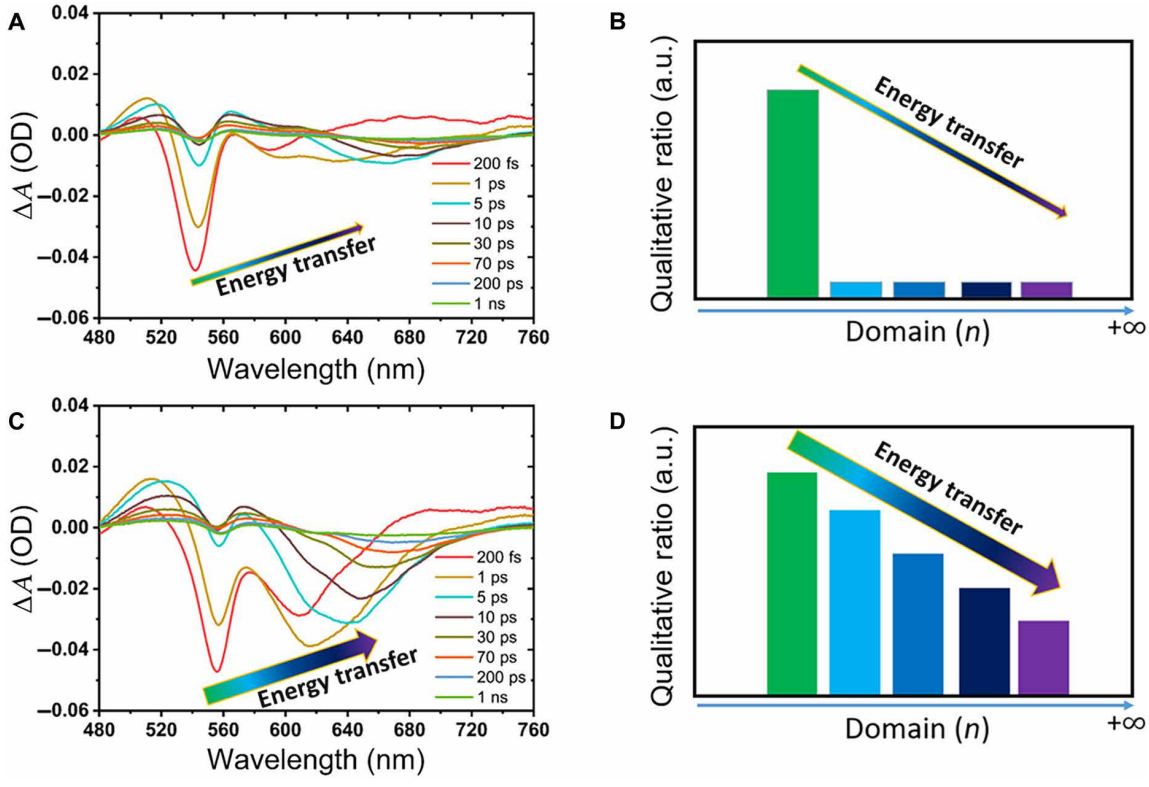

Fig. 4. TA spectra of DJ structure perovskite films. TA spectra of (**A**) **BAB33** and (**C**) **BAB25** perovskite film. Scheme of the qualitative ratio of components with varied *n* value in (**B**) **BAB33** and (**D**) **BAB25** perovskite film and energy transfer process. The direction of the arrow represents the energy transfer. The relative ratio of multilayered structure and the energy transfer efficiency are increased as the decrease in BAB ratio. OD, optical density.

are selected to align the energy levels of perovskite film. We obtained the band structure of **BAB25** film by combining ultraviolet (UV) photoelectron spectrum (UPS) and absorption spectra. The cutoff sideband in UPS is located at 17.34 eV, corresponding to a work function of −3.88 eV; in combination with the offset value of 1.38 eV, the valence band is determined to be −5.26 eV. On the basis of the cutoff position of the absorption spectrum, the minimum conduction band position is calculated to be −3.67 eV (fig. S9, E and F). We used ZnO nanocrystal film as an electron-transporting layer due to its high electron mobility. A monolayer of PEIE was coated on the ZnO film to improve surface coverage and modify work function (−3.7 eV) for more efficient carrier injection (*33*, *34*). TFB with the highest occupied molecular orbital level of −5.4 eV was used as hole-transporting and electron-blocking layer on top of the emission layer (*35*). The thickness of ZnO/PEIE, perovskite, and TFB is about 30, 280, and 50 nm, respectively (fig. S10A).

We then characterize the performance of the LED based on DJ structural perovskites. The electroluminescence spectra of the perovskite LEDs with different BAB ratios are shown in Fig. 5B. As the increase in BAB ratio, the emission peaks are blue-shifted from 787 to 731 nm. The emission peak of the **BAB25** is located at 776 nm with an FWHM of 50 nm. The peak position of the electroluminescence spectrum is red-shifted, relative to the PL spectrum in Fig. 2B, owing to carrier transfer from perovskite of large bandgap to small ones, as shown in TAS study (Fig. 4). Electric field–induced Stark effect is another potential factor (*36*).

Figure 5C shows the current density–voltage and radiance-voltage characteristics of the device based on various BAB ratios. The leakage current is well suppressed thanks to homogeneous smooth surface topography (fig. S5). The best device exhibits a low turn-on voltage of approximately 1.2 V, even lower than the photon voltage corresponding to the optical bandgap of DJ structure perovskite ($h\nu \approx 1.6$ eV). This can be attributed to the Auger-assisted energy up-conversion process in devices containing colloidal ZnO nanoparticles as electron transport layers (*37*, *38*). The current density and radiance increase sharply once the voltage reaches the threshold voltage, demonstrating a low series resistance and efficient carrier injection into the device. The performance of DJ structure perovskite LEDs with different BAB are shown in Table 1. The maximum radiant intensity is 88.5 W sr^{-1} m^{-2} at 5.5 V. The peak EQE of 5.20% is realized at a radiance intensity of 15.44 W sr^{-1} m^{-2} (Fig. 5D) under a current density of 77.73 mA cm^{-2}. To evaluate the reproducibility of the performance of the DJ structure perovskite device, a statistical histogram of 52 device performance is shown in fig. S10C, and the average peak EQE is 4.2%. The relatively high EQE can be maintained in a wide range of current densities, and it is more than 3% when the current density is in the range of 10 to 742 mA cm^{-2}. The low efficiency roll-off is superior to most of the reported perovskite

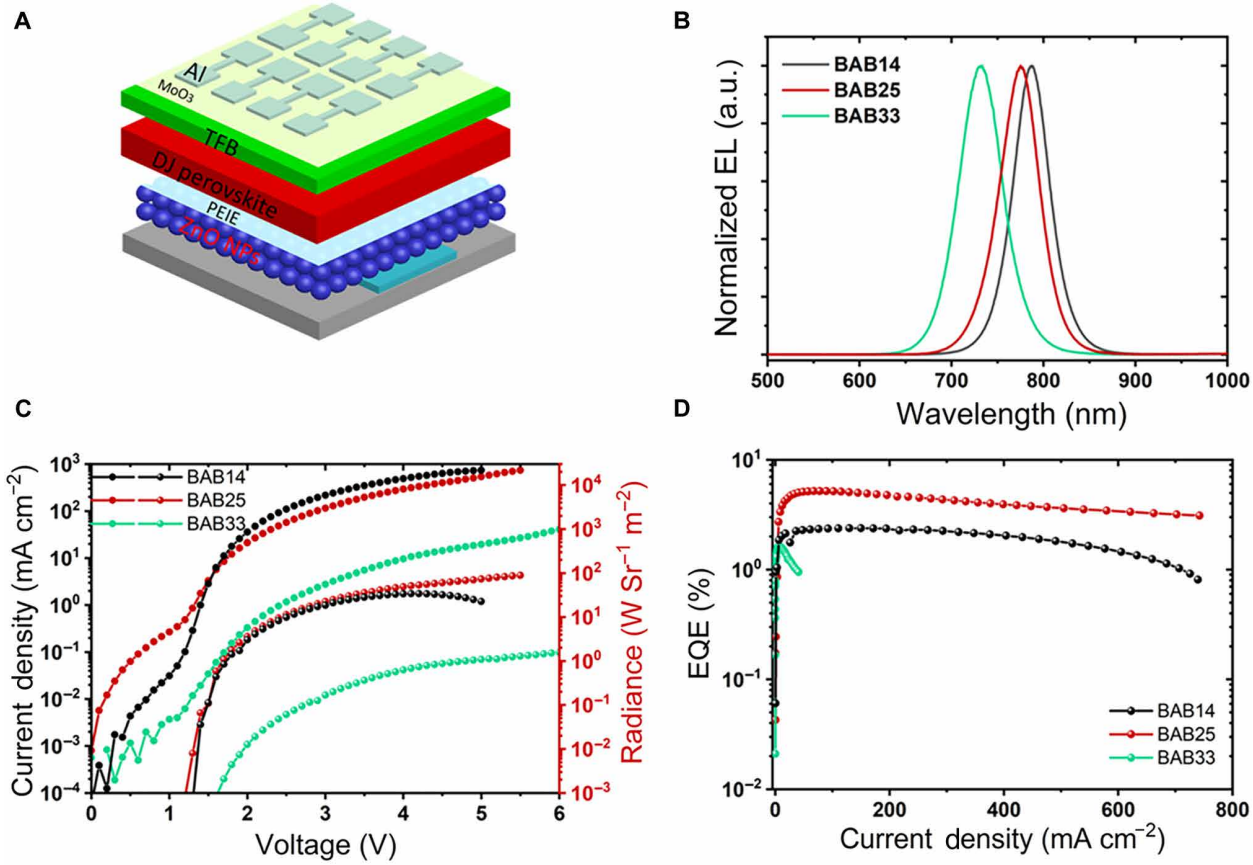

Fig. 5. Characteristics of DJ structure perovskite LEDs. (**A**) Device structure. (**B**) Normalized electroluminescence spectra of hybrid DJ structure perovskite LEDs with varied ligand additive. (**C**) Current density–voltage-radiance curves and (**D**) EQE curve of hybrid DJ structure perovskite LEDs.

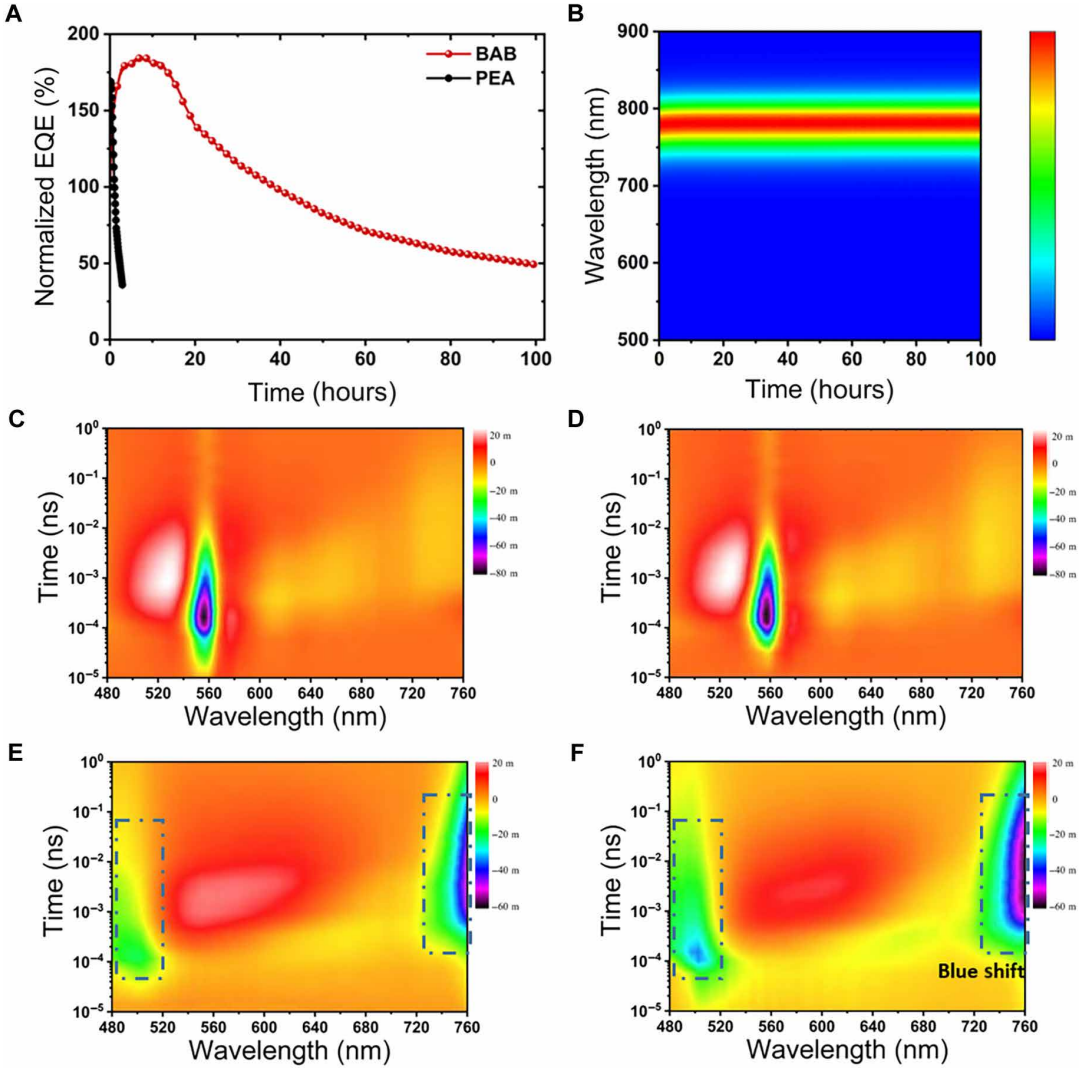

Fig. 6. Stability analysis of DJ structure perovskite LEDs. (**A**) Operational lifetimes and (**B**) peak position of DJ structure perovskite–based LEDs at a constant current density of 25 mA cm^{-2} for 100 hours. (**C** and **D**) TAS of BAB-based DJ structure perovskite film before and after continuous operation. (**E** and **F**) TAS of PEA-based RP structure perovskite film before and after continuous operation. The intensity of the bleaching peak at 485 nm is increased, and the peak at 770 nm is slightly blue shifted.

LED devices based on hybrid perovskite structure and much better than that based on colloidal perovskite nanoparticles (*17*).

To further investigate the stability of the DJ structural perovskite LEDs, we tracked the efficiency of the unencapsulated devices in a N_2-filled glovebox. Driven by a fixed current of 25 mA cm^{-2} that generates the highest EQE value, the EQE value of the device remains over 50% of its original value after continuous operation for 100 hours. Furthermore, the electroluminescence spectra and the peak position of the device-based DJ structure are identical during 100 hours of stability tracking (Fig. 6B). In contrast, a control device based on typical RP structure shows T_{50} value of only 3 hours. The increase in EQE in the beginning can be attributed to electric field boiling induced defect reduction (Fig. 6A) (*39*). Since the luminescence efficiency is much less than unity, much energy will change into heat during device operation. This could cause the recrystallization of the film and cure part defects. Furthermore, ion moving in the film could bring ion doping of carrier-transporting layer, improving carrier injection into perovskite. The slow decay of device performance in long-term operation could be related to interfacial degradation between active and carrier-transporting layers due to ions accumulation (*40*).

Table 1. The summary of DJ structure perovskite LED performance with varied BAB ratios.

BAB	Max radiance (W sr^{-1} m^{-2})	Max EQE (%)	Average EQE (%)
14%	1.58	1.63	1.2
25%	88.5	5.2	4.2
33%	33.9	2.42	1.8

To analyze the mechanism for the enhanced stability of DJ structure–based device under the continuous driving of the electric field, we used TA measurement to track the composition of the films after continuous operation. The device with DJ structure

showed identical excitation peaks before and after stability measurement (Fig. 6, C and D), whereas a remarkable change of spectra was found for the film based on RP structure (Fig. 6, E and F). First, the intensity of the bleaching peak at 500 nm that related to PbI_2 or low-dimensional perovskite structure is increased, which can be caused by decomposition of perovskite structure (fig. S13C). The lifetime of this peak is increased after operation, which can possibly be explained by the decrease in carrier transfer efficiency to perovskite structure. Furthermore, the peak at 770 nm deriving from 3D structure perovskite is slightly blue-shifted (fig. S13D), implying the decomposition of perovskite structure as well. We thereby conclude that DJ structure was kept well after long-term operation, while RP structure was remarkably changed.

DISCUSSION

In summary, we performed a combined theoretical and experimental study to increase the stability of perovskite LED using DJ structure. Theoretical simulation indicates that the DJ structural perovskite has a higher decomposition energy than the RP structural one. The formation of DJ structure using BAB as bridging ligands is confirmed by GIWAXS measurement and TA study. The optimized DJ structural perovskite film exhibits the best EQE of 5.20% with a maximum radiance of 88.5 W sr^{-1} m^{-2}. The EQE roll-off is significantly reduced, and the device shows the operating lifetime of 100 hours, almost two orders of magnitude longer compared with RP structure. This is the longest T_{50} value reported up to now for hybrid perovskite that tested at the current density, giving rise to the best EQE value. In situ TA measurement showed that the perovskite structure was kept well after long-term operation, proving that DJ structure can effectively improve the stability of perovskite films. This work extends the kinds of low-dimensional structures that can be applied for LEDs and indicates that the quantum well distribution regulated DJ film is a promising structure for pursuing robust and efficient perovskite LED devices.

MATERIALS AND METHODS

Materials

N,*N*′-dimethylformamide (DMF; 99.8%), dimethyl sulfoxide (DMSO; 99.9%), hydrobromic acid [HBr; 48 weight % (wt %) in water], BAB (99%), and polyethylenimine (80% ethoxylated solution and 37 wt % in H_2O) were purchased from Sigma-Aldrich. PbI_2 (99.99%; trace metals basis) was purchased from Tokyo Chemical Industry (TCI). TFB (99.8%) and FAI (≥99.5%) were purchased from Xi'an p-OLED company. Zinc acetate dihydrate (99.99%) and tetramethylammonium hydroxide pentahydrate (TMAH; 97%) were purchased from Aladdin Reagents. All other organic solvents were purchased from Aladdin Reagents. All chemicals were used directly without any further purification, unless otherwise stated.

Synthesis of $BABBr_2$

BAB (2.724 g, 20 mmol) was dissolved in 20 ml of ethanol in an ice bath, and HBr aqueous solution (48 wt %, 9 ml, 80 mmol) was added dropwise to the flask with vigorous stirring. Subsequently, the mixture was allowed to stand in ice bath for another half hour. The precipitate was filtered under vacuum and washed thoroughly using cold diethyl ether.

Synthesis of ZnO nanoparticles

ZnO nanoparticles were synthesized using a solution-precipitation process reported previously (*41*). Briefly, zinc acetate dihydrate (1.308 g, 6 mmol) was dissolved in 60 ml of DMSO, forming a colorless transparent solution. Then, TMAH (1.68 g, 9 mmol) mixed with 20 ml of ethanol was added dropwise into the zinc acetate solution and stirred for 4 hours in ambient air. The ZnO nanoparticles were centrifuged and washed with ethyl acetate twice, and 80 μl of ethanolamine was added during the second cleaning process. Last, ZnO nanoparticles were dispersed in ethanol, forming a transparent solution with a concentration of 10 mg ml^{-1}.

Preparation of perovskite precursor solution

The (BAB) $FA_{n-1}Pb_nX_{3n+1}$ precursor solution was prepared by mixing $BABBr_2$, FAI, and PbI_2 with a molar ratio of 1:2:3 or 1:3:3 in DMF (35 wt %) that were stirred at room temperature for 12 hours in a glovebox.

Device fabrication and characterization

The ITO-coated glass substrates (10 ohms per square) were cleaned consecutively with Triton X-100 solution, isopropanol, and deionized water under sonication for 15 min each and were then treated with O_2 plasma for 15 min. Subsequently, the substrates were spin-coated with ZnO nanoparticles solution (10 mg ml^{-1}) and baked at 120°C for 15 min in air. Then, the substrates transferred into a N_2-filled glovebox for the device fabrication. The ultrathin layer of PEIE films was prepared following the reported method (*34*). For the DJ structure perovskite films, the precursor was spin-coated onto the PEIE-treated ZnO films at 3000 rpm for 60 s, followed by baking at 100°C for 10 min. The TFB layers were deposited from a chlorobenzene solution (6 mg ml^{-1}) at 2000 rpm. Last, MoO_3 (8 nm) and Al (120 nm) electrodes were deposited by thermal evaporation under a based vacuum of ~2×10^{-7} torr. The effective area of devices is 5 mm^2 as defined by the overlapping area of the ITO films and top electrodes.

The current density–luminance-radiance (*J*-*V*-*R*) characteristics were acquired by a Keithley 2400 source meter and a fiber integrating sphere (FOIS-1) couple with a QE Pro650 spectrometer (Ocean Optics). The LED devices were tested on top of the integrating sphere, and only forward light emission could be collected, which is consistent with the standard OLED characterization method. All of the device test processes were performed in the N_2-filled glovebox.

Film characterization

Optical absorbance was measured with an Agilent Cary 5000 spectrometer, and Flog-3 (HORIBA) was used to characterize the film PL, PL QY, and PL excitation spectra. The PL decay experiments were performed on the same samples using the same Fluorolog with a pulsed source at 408 nm (HORIBA NanoLED 405-LH), and the signal was recorded using Time-Correlated Single Photon Counting (TCSPC). TA was measured using a HELIOS femtosecond transient absorption spectrometer (Ultrafast Systems LLC) with a 450-nm laser (140 mJ cm^{-2}). In situ fluorescence spectra were recorded using a USB2000+ spectrometer (Ocean Optics) with a 200-mm optical fiber in a N_2-filled glovebox, and the excited light was at 390 nm from a UV lamp. The atomic force microscopy (AFM) surface morphology of the films was measured using the Bruker AFM system (FastSCAN). The ZnO nanoparticles were characterized using a JEOL-2100Plus transmission electron microscope with a 120-keV electron beam energy. The XRD characterizations were taken on a Bruker D8 system using Cu Kα (λ = 1.5405 Å) as the x-ray source and x-ray generator settings at 40 kV

and 30 mA, respectively. X-ray photoemission spectroscopy (XPS) and UPS data were conducted using an ESCALAB 250Xi (Thermo Fisher Scientific). A monochromatic Al Kα line (1486.6 eV) was used for XPS, and He-I radiation (21.22 eV) with an applied bias of −10 V was used for UPS.

GIWAXS studies were performed at the BL16B1 beamline of Shanghai Synchrotron Radiation Facility, Shanghai, China using a beam energy of 10 keV (λ = 1.2398 Å) and a Mar 225 detector. Images were acquired with a 50-s (for 33, 50, and 100% samples) or 100-s (for FAI additive samples) exposure time. The distance between the sample and detector was 220 mm. The grazing incidence angles for all films were 0.1°, 0.2°, 0.5°, 1°, and 2°, respectively. The GIXSGUI (MATLAB toolbox) was used to analyze the raw patterns (*42*).

First-principles calculations

First-principles calculations were performed within the framework of DFT using plane-wave pseudopotential methods as implemented in the Vienna Ab initio Simulation Package (*43*, *44*). The generalized gradient approximation formulated by Perdew *et al.* (*45*) was used as the exchange-correlation functional. The electron-core interactions were described by the projector augmented-wave (*46*) method for the pseudopotentials. The cutoff energy for the plane-wave basis set used to expand the Kohn-Sham orbitals was 520 eV. In addition, the gamma-centered *k*-point mesh with grid spacing of $2\pi \times 0.03$ Å^{-1} was used for electronic Brillouin zone integration. The equilibrium structural parameters (including both lattice parameters and internal coordinates) of each involved material were obtained via total energy minimization using the conjugate-gradient algorithm, with the force convergence threshold of 0.01 eV Å^{-1}. The optB86b-vdW (*47*) functional was adopted to get proper lattice parameters.

SUPPLEMENTARY MATERIALS

Supplementary material for this article is available at http://advances.sciencemag.org/cgi/content/full/5/8/eaaw8072/DC1

Details for DFT simulations
Fig. S1. Structures used in DFT simulations.
Fig. S2. Binding energy calculation.
Fig. S3. Structures used in molecule dissociation energy calculation.
Fig. S4. Density of states and band structure.
Fig. S5. Surface roughness of perovskite films.
Fig. S6. XRD pattern of the DJ structure perovskite with **BAB33**.
Fig. S7. GIWAXS pattern of DJ structure perovskite films.
Fig. S8. TA spectra study.
Fig. S9. XPS and UPS of the DJ structure perovskite.
Fig. S10. Perovskite film thickness and device statistics.
Fig. S11. Device performance in ambient air.
Fig. S12. In situ PL study.
Fig. S13. Stability analysis.
Table S1. The summarized crystal structure parameters of various calculated perovskite phases.
Table S2. The summarized binding energy of the perovskite based on different ligands.
Table S3. The summarized perovskite LED stability.

REFERENCES AND NOTES

1. L. N. Quan, F. P. Garcia de Arquer, R. P. Sabatini, E. H. Sargent, Perovskites for light emission. *Adv. Mater.* **30**, 1801996 (2018).
2. Y.-H. Kim, H. Cho, T.-W. Lee, Metal halide perovskite light emitters. *Proc. Natl. Acad. Sci. U.S.A.* **113**, 11694–11702 (2016).
3. M. Yuan, L. N. Quan, R. Comin, G. Walters, R. Sabatini, O. Voznyy, S. Hoogland, Y. Zhao, E. M. Beauregard, P. Kanjanaboos, Z. Lu, D. H. Kim, E. H. Sargent, Perovskite energy funnels for efficient light-emitting diodes. *Nat. Nanotechnol.* **11**, 872–877 (2016).
4. N. N. Wang, L. Cheng, R. Ge, S. Zhang, Y. Miao, W. Zou, C. Yi, Y. Sun, Y. Cao, R. Yang, Y. Wei, Q. Guo, Y. Ke, M. Yu, Y. Jin, Y. Liu, Q. Ding, D. Di, L. Yang, G. Xing, H. Tian, C. Jin, F. Gao, R. H. Friend, J. Wang, W. Huang, Perovskite light-emitting diodes based on solution-processed self-organized multiple quantum wells. *Nat. Photonics* **10**, 699–704 (2016).
5. Y. Ling, Y. Tian, X. Wang, J. C. Wang, J. M. Knox, F. Perez-Orive, Y. Du, L. Tan, K. Hanson, B. Ma, H. Gao, Enhanced optical and electrical properties of polymer-assisted all-inorganic perovskites for light-emitting diodes. *Adv. Mater.* **28**, 8983–8989 (2016).
6. Y. Shang, G. Li, W. Liu, Z. Ning, Quasi-2D inorganic $CsPbBr_3$ perovskite for efficient and stable light-emitting diodes. *Adv. Funct. Mater.* **28**, 1801193 (2018).
7. J. Byun, H. Cho, C. Wolf, M. Jang, A. Sadhanala, R. H. Friend, H. Yang, T.-W. Lee, Efficient visible quasi-2D perovskite light-emitting diodes. *Adv. Mater.* **28**, 7515–7520 (2016).
8. H. Cho, S.-H. Jeong, M.-H. Park, Y.-H. Kim, C. Wolf, C.-L. Lee, J. H. Heo, A. Sadhanala, N. Myoung, S. Yoo, S. H. Im, R. H. Friend, T.-W. Lee, Overcoming the electroluminescence efficiency limitations of perovskite light-emitting diodes. *Science* **350**, 1222–1225 (2015).
9. Y.-H. Kim, J. S. Kim, T.-W. Lee, Strategies to improve luminescence efficiency of metal-halide perovskites and light-emitting diodes. *Adv. Mater.* **2018**, 1804595 (2018).
10. X. Y. Chin, D. Cortecchia, J. Yin, A. Bruno, C. Soci, Lead iodide perovskite light-emitting field-effect transistor. *Nat. Commun.* **6**, 7383 (2015).
11. G. Rainò, M. A. Becker, M. I. Bodnarchuk, R. F. Mahrt, M. V. Kovalenko, T. Stöferle, Superfluorescence from lead halide perovskite quantum dot superlattices. *Nature* **563**, 671–675 (2018).
12. H. Kim, L. Zhao, J. S. Price, A. J. Grede, K. Roh, A. N. Brigeman, M. Lopez, B. P. Rand, N. C. Giebink, Hybrid perovskite light emitting diodes under intense electrical excitation. *Nat. Commun.* **9**, 4893 (2018).
13. Z. Chen, Z. Li, C. Zhang, X.-F. Jiang, D. Chen, Q. Xue, M. Liu, S. Su, H.-L. Yip, Y. Cao, Recombination dynamics study on nanostructured perovskite light-emitting devices. *Adv. Mater.* **30**, 1801370 (2018).
14. Y. Cao, N. Wang, H. Tian, J. Guo, Y. Wei, H. Chen, Y. Miao, W. Zou, K. Pan, Y. He, H. Cao, Y. Ke, M. Xu, Y. Wang, M. Yang, K. Du, Z. Fu, D. Kong, D. Dai, Y. Jin, G. Li, H. Li, Q. Peng, J. Wang, W. Huang, Perovskite light-emitting diodes based on spontaneously formed submicrometre-scale structures. *Nature* **562**, 249–253 (2018).
15. K. Lin, J. Xing, L. N. Quan, F. P. G. de Arquer, X. Gong, J. Lu, L. Xie, W. Zhao, D. Zhang, C. Yan, W. Li, X. Liu, Y. Lu, J. Kirman, E. H. Sargent, Q. Xiong, Z. Wei, Perovskite light-emitting diodes with external quantum efficiency exceeding 20 per cent. *Nature* **562**, 245–248 (2018).
16. B. Zhao, S. Bai, V. Kim, R. Lamboll, R. Shivanna, F. Auras, J. M. Richter, L. Yang, L. Dai, M. Alsari, X.-J. She, L. Liang, J. Zhang, S. Lilliu, P. Gao, H. J. Snaith, J. Wang, N. C. Greenham, R. H. Friend, D. Di, High-efficiency perovskite-polymer bulk heterostructure light-emitting diodes. *Nat. Photonics* **12**, 783–789 (2018).
17. T. Chiba, Y. Hayashi, H. Ebe, K. Hoshi, J. Sato, S. Sato, Y.-J. Pu, S. Ohisa, J. Kido, Anion-exchange red perovskite quantum dots with ammonium iodine salts for highly efficient light-emitting devices. *Nat. Photonics* **12**, 681–687 (2018).
18. Z.-K. Tan, R. S. Moghaddam, M. L. Lai, P. Docampo, R. Higler, F. Deschler, M. Price, A. Sadhanala, L. M. Pazos, D. Credgington, F. Hanusch, T. Bein, H. J. Snaith, R. H. Friend, Bright light-emitting diodes based on organometal halide perovskite. *Nat. Nanotechnol.* **9**, 687–692 (2014).
19. G. Divitini, S. Cacovich, F. Matteocci, L. Cinà, A. Di Carlo, C. Ducati, In situ observation of heat-induced degradation of perovskite solar cells. *Nat. Energy* **1**, 15012 (2016).
20. J. Huang, S. Tan, P. D. Lund, H. Zhou, Impact of H_2O on organic-inorganic hybrid perovskite solar cells. *Energy Environ. Sci.* **10**, 2284–2311 (2017).
21. C. C. Boyd, R. Cheacharoen, T. Leijtens, M. D. McGehee, Understanding degradation mechanisms and improving stability of perovskite photovoltaics. *Chem. Rev.* **119**, 3418–3451 (2019).
22. Z. Li, C. Xiao, Y. Yang, S. P. Harvey, D. H. Kim, J. A. Christians, M. Yang, P. Schulz, S. U. Nanayakkara, C.-S. Jiang, J. M. Luther, J. J. Berry, M. C. Beard, M. M. Al-Jassim, K. Zhu, Extrinsic ion migration in perovskite solar cells. *Energy Environ. Sci.* **10**, 1234–1242 (2017).
23. E. T. Hoke, D. J. Slotcavage, E. R. Dohner, A. R. Bowring, H. I. Karunadasa, M. D. McGehee, Reversible photo-induced trap formation in mixed-halide hybrid perovskites for photovoltaics. *Chem. Sci.* **6**, 613–617 (2015).
24. C. Eames, J. M. Frost, P. R. F. Barnes, B. C. O'Regan, A. Walsh, M. S. Islam, Ionic transport in hybrid lead iodide perovskite solar cells. *Nat. Commun.* **6**, 7497 (2015).
25. Y. Tian, C. Zhou, M. Worku, X. Wang, Y. Ling, H. Gao, Y. Zhou, Y. Miao, J. Guan, B. Ma, Highly efficient spectrally stable red perovskite light-emitting diodes. *Adv. Mater.* **30**, 1707093 (2018).
26. Y. Li, J. V. Milic, A. Ummadisingu, J.-Y. Seo, J.-H. Im, H. S. Kim, Y. Liu, M. I. Dar, S. M. Zakeeruddin, P. Wang, A. Hagfeldt, M. Gratzel, Bifunctional organic spacers for formamidinium-based hybrid Dion-Jacobson two-dimensional perovskite solar cells. *Nano Lett.* **19**, 150–157 (2019).
27. L. Mao, W. Ke, L. Pedesseau, Y. Wu, C. Katan, J. Even, M. R. Wasielewski, C. C. Stoumpos, M. G. Kanatzidis, Hybrid Dion-Jacobson 2D lead iodide perovskites. *J. Am. Chem. Soc.* **140**, 3775–3783 (2018).

28. S. Ahmad, P. Fu, S. Yu, Q. Yang, X. Liu, X. Wang, X. Wang, X. Guo, C. Li, Dion-Jacobson phase 2D layered perovskites for solar cells with ultrahigh stability. *Joule* **3**, 794–806 (2019).
29. F. Wang, W. Geng, Y. Zhou, H.-H. Fang, C.-J. Tong, M. A. Loi, L.-M. Liu, N. Zhao, Phenylalkylamine passivation of organolead halide perovskites enabling high-efficiency and air-stable photovoltaic cells. *Adv. Mater.* **28**, 9986–9992 (2016).
30. R. Grisorio, M. E. Di Clemente, E. Fanizza, I. Allegretta, D. Altamura, M. Striccoli, R. Terzano, C. Giannini, M. Irimia-Vladu, G. P. Suranna, Exploring the surface chemistry of cesium lead halide perovskite nanocrystals. *Nanoscale* **11**, 986–999 (2019).
31. B.-E. Cohen, Y. Li, Q. Meng, L. Etgar, Dion-Jacobson two-dimensional perovskite solar cells based on benzene dimethanammonium cation. *Nano Lett.* **19**, 2588–2597 (2019).
32. Y. Hassan, Y. Song, R. D. Pensack, A. I. Abdelrahman, Y. Kobayashi, M. A. Winnik, G. D. Scholes, Structure-tuned lead halide perovskite nanocrystals. *Adv. Mater.* **28**, 566–573 (2016).
33. Y. Zhou, C. Fuentes-Hernandez, J. Shim, J. Meyer, A. J. Giordano, H. Li, P. Winget, T. Papadopoulos, H. Cheun, J. Kim, M. Fenoll, A. Dindar, W. Haske, E. Najafabadi, T. M. Khan, H. Sojoudi, S. Barlow, S. Graham, J.-L. Brédas, S. R. Marder, A. Kahn, B. Kippelen, A universal method to produce low-work function electrodes for organic electronics. *Science* **336**, 327–332 (2012).
34. J. Wang, N. Wang, Y. Jin, J. Si, Z.-K. Tan, H. Du, L. Cheng, X. Dai, S. Bai, H. He, Z. Ye, M. L. Lai, R. H. Friend, W. Huang, Interfacial control toward efficient and low-voltage perovskite light-emitting diodes. *Adv. Mater.* **27**, 2311–2316 (2015).
35. G. M. Lazzerini, F. Di Stasio, C. Fléchon, D. J. Caruana, F. Cacialli, Low-temperature treatment of semiconducting interlayers for high-efficiency light-emitting diodes based on a green-emitting polyfluorene derivative. *Appl. Phys. Lett.* **99**, 243305 (2011).
36. J.-M. Caruge, J. E. Halpert, V. Bulović, M. G. Bawendi, NiO as an inorganic hole-transporting layer in quantum-dot light-emitting devices. *Nano Lett.* **6**, 2991–2994 (2006).
37. L. Qian, Y. Zheng, K. R. Choudhury, D. Bera, F. So, J. Xue, P. H. Holloway, Electroluminescence from light-emitting polymer/ZnO nanoparticle heterojunctions at sub-bandgap voltages. *Nano Today* **5**, 384–389 (2010).
38. L. Qian, Y. Zheng, J. Xue, P. H. Holloway, Stable and efficient quantum-dot light-emitting diodes based on solution-processed multilayer structures. *Nat. Photonics* **5**, 543–548 (2011).
39. C.-C. Zhang, Z.-K. Wang, M. Li, Z.-Y. Liu, J.-E. Yang, Y.-G. Yang, X.-Y. Gao, H. Ma, Electric-field assisted perovskite crystallization for high-performance solar cells. *J. Mater. Chem. A* **6**, 1161–1170 (2018).
40. T. A. Berhe, W.-N. Su, C.-H. Chen, C.-J. Pan, J.-H. Cheng, H.-M. Chen, M.-C. Tsai, L.-Y. Chen, A. A. Dubale, B.-J. Hwang, Organometal halide perovskite solar cells: Degradation and stability. *Energy Environ. Sci.* **9**, 323–356 (2016).
41. Y. Yang, Y. Zheng, W. Cao, A. Titov, J. Hyvonen, J. R. Manders, J. Xue, P. H. Holloway, L. Qian, High-efficiency light-emitting devices based on quantum dots with tailored nanostructures. *Nat. Photonics* **9**, 259–266 (2015).
42. Z. Jiang, *GIXSGUI*: A MATLAB toolbox for grazing-incidence X-ray scattering data visualization and reduction, and indexing of buried three-dimensional periodic nanostructured films. *J. Appl. Crystallogr.* **48**, 917–926 (2015).
43. G. Kresse, J. Furthmuller, Efficient iterative schemes for ab initio total-energy calculations using a plane-wave basis set. *Phys. Rev. B* **54**, 11169–11186 (1996).
44. G. Kresse, J. Furthmuller, Efficiency of ab-initio total energy calculations for metals and semiconductors using a plane-wave basis set. *Comput. Mater. Sci.* **6**, 15–50 (1996).
45. J. P. Perdew, K. Burke, M. Ernzerhof, Generalized gradient approximation made simple. *Phys. Rev. Lett.* **77**, 3865–3868 (1996).
46. P. E. Blöchl, Projector augmented-wave method. *Phys. Rev. B* **50**, 17953–17979 (1994).
47. J. Klimeš, D. R. Bowler, A. Michaelides, Van der Waals density functionals applied to solids. *Phys. Rev. B* **83**, 195131 (2011).

Acknowledgments: We thank Z. Xiu and P. Cheng for help in the device fabrication. We also thank the Test Center of ShanghaiTech University and the HPC Platform of ShanghaiTech University. **Funding:** This work was supported by the Shanghai International Cooperation Project (16520720700), Shanghai Key Research Program (16JC1402100), ShanghaiTech Start-up Funding, 1000 Young Talent Program, and National Natural Science Foundation of China (U1632118 and 21571129). **Author contributions:** Z.N. and Y.S. conceived the idea and planned the experiments. Y.S. and Y.L. conducted most of the device fabrication, measurement, and characterization. Q.W. and Y.K. performed the DFT simulations. Z.W. and W.L. contributed to the TAS study. B.X. synthesized the ZnO nanoparticles. Z.N. and Y.S. wrote the manuscript. All authors discussed the results and revised the manuscript. **Competing interests:** The authors declare that they have no competing interests. **Data and materials availability:** All data needed to evaluate the conclusions in the paper are present in the paper and/or the Supplementary Materials. Additional data related to this paper may be requested from the authors.

Submitted 26 January 2019
Accepted 8 July 2019
Published 16 August 2019
10.1126/sciadv.aaw8072

Citation: Y. Shang, Y. Liao, Q. Wei, Z. Wang, B. Xiang, Y. Ke, W. Liu, Z. Ning, Highly stable hybrid perovskite light-emitting diodes based on Dion-Jacobson structure. *Sci. Adv.* **5**, eaaw8072 (2019).

Highly stable hybrid perovskite light-emitting diodes based on Dion-Jacobson structure

Yuequn Shang, Yuan Liao, Qi Wei, Ziyu Wang, Bo Xiang, Youqi Ke, Weimin Liu and Zhijun Ning

Sci Adv **5** (8), eaaw8072.
DOI: 10.1126/sciadv.aaw8072